RESEARCH MEMORANDUM

for the

Armed Forces, Special Weapons Project

INVESTIGATION OF THE ATTENUATION OF PLANE SHOCK WAVES MOVING OVER VERY ROUGH SURFACES

By Paul W. Huber, Donald R. McFarland, and Philip Levine

Langley Aeronautical Laboratory
Langley Field, Va.

NATIONAL ADVISORY COMMITTEE
FOR AERONAUTICS

WASHINGTON

NACA RM SL53D13a

NATIONAL ADVISORY COMMITTEE FOR AERONAUTICS

RESEARCH MEMORANDUM

for the

Armed Forces, Special Weapons Project

INVESTIGATION OF THE ATTENUATION OF PLANE SHOCK WAVES MOVING OVER VERY ROUGH SURFACES

By Paul W. Huber, Donald R. McFarland, and Philip Levine

SUMMARY

Experimental measurements of the attenuation of plane shock waves moving over rough walls have been made in a shock tube. Measurements of the boundary-layer characteristics, including thickness and velocity distribution behind the shock, have also been made with the aid of new optical techniques which provide direct information on the local boundary-layer conditions at the rough walls. Measurements of shock speed and shock pressure ratio are presented for both smooth-wall and rough-wall flow over lengths of machined-smooth and rough strips which lined all four walls of the shock tube. A simplified theory based on Von Kármán's expression for skin-friction coefficient for flow over rough walls, along with a wave-model concept and extensions to include time effects, is presented. In this theory, the shock-tube flow is assumed to be one-dimensional at all times and the wave-model concept is used to relate the local boundary-layer growth to decreases in shock strength. This concept assumes that local boundary-layer growths act as local mass-flow sinks, which give rise to expansion waves which, in turn, overtake the shock and lower its mass flow accordingly.

The results show that while agreement of boundary-layer measurements is good for all shock strengths, and while agreement of shock-attenuation measurements with theory is good for all the shock strengths in the smooth-wall case, the agreement of attenuation measurements with theory for the stronger shocks is poor in the rough-wall case. Discussions are presented which qualitatively account for this discrepancy in terms of distortions of the assumed one-dimensional wave model.

INTRODUCTION

There are no existing theories or experimental data which could be used to determine what attenuation might be expected with shock waves

moving over very rough surfaces. Some previous investigations have shown, by means of schlieren photographs, distortions of the shock near rough walls as well as the growth of a rather thick boundary layer along the wall. Investigations have also been made of the diffraction of waves about various-shaped bodies. In general, these data are only qualitative with regard to the shock strength as a function of time, distance, and surface conditions.

To represent this type of flow with an exact theory would, of course, be exceedingly difficult if not impossible. In order to construct any theoretical model of this flow the problem must be highly idealized, in which case its applicability is usually quite limited.

To transform the system directly to any stationary coordinates, such as flat-plate theory or impulsively actuated plate theory, would be a questionable procedure since in neither case is time allowed to sweep the plate, as it is in the actual case. The transfer of intelligence from the boundary layer to the shock is a process of great time dependence also. Three-dimensionality of the surface and the resulting wave diffraction pattern, as well as heat-transfer effects, all lead to great complication of the problem.

In order to construct an experimental and theoretical model, even though highly idealized, from which comparisons might be made, the boundary-layer mass-flow sink concept from Donaldson and Sullivan (ref. 1) was used, along with Von Kármán's work on skin-friction coefficients for rough surfaces (ref. 2), as a starting point. From this starting point, which was first suggested by Donaldson (ref. 1), and with corrections introduced to account for time of intelligence transfer from boundary layer to shock, an investigation was begun using the shock-tube facilities of the Langley gas dynamics laboratory. During the course of the investigation a method using bullets was developed from which the boundary-layer height and velocity distribution at the rough wall could be determined.

SYMBOLS

a	acoustic velocity
A	cross-sectional area; roughness constant
B	roughness constant
c_f	local coefficient of friction

C_f mean coefficient of friction

D perimeter of inside of shock tube

k roughness height

L distance from leading edge of wall to measuring station

m mass flow

M Mach number, u/a

N velocity-profile power

P pressure

R_x Reynolds number based on x

S_1 shock velocity

t time

u local velocity

x flow distance from leading edge of wall

y coordinate of boundary-layer height

α angle between flow direction and a line tangent to bullet wave

$\beta = \frac{\delta^*}{\delta}$

$\eta = \frac{\delta}{\theta}$

δ^* boundary-layer displacement thickness

θ boundary-layer momentum thickness

δ nominal boundary-layer thickness

ϕ shock strength, P_2/P_1

Subscripts:

o high-pressure side of diaphragm

1 undisturbed conditions existing in tube ahead of shock wave

2	flow quantities in rear of shock-tube shock wave
n	Mach number of relative flow normal to wave from bullet
T	bullet wave relative to stream
w	flow quantities at wall
b	bullet wave relative to wall
max	maximum

THEORETICAL METHOD

In reference 1, the assumption was made that the boundary layer behind the shock wave, because of its growing displacement thickness, acts as a mass-flow sink and reduces the strength of the shock wave to correspond to the lower mass flow by the mechanism of expansion waves originating at the boundary layer and catching the shock, thereby weakening it. The same mechanism is herein used in calculating the shock attenuation due to smooth and rough walls for the case of turbulent flow, except that the time of travel of the expansion waves is included. The prediction of boundary-layer growth for both smooth and rough walls was taken from Von Kármán's work on skin-friction coefficients (ref. 2). The method herein used also assumes a one-dimensional wave model as in reference 1. Wave diffraction effects are also neglected in this work, since in the one-dimensional case for small area changes the loss in wave strength is insignificant in departing from and coming back to the original area.

Von Kármán's work shows essentially that in the case of very rough walls where the roughness heights are large compared with the thickness of a calculated smooth-wall laminar boundary layer, the boundary layer is a function only of the ratio δ/k. That is, the dependence of rough-wall boundary layers is primarily on the roughness height and not on the Reynolds number, as is the case for smooth walls.

For the smooth-wall case and turbulent flow (ref. 2)

$$\delta = 0.38 x C_f^{1/2} \tag{1}$$

$$\frac{1}{C_f^{1/2}} = 1.7 + 4.15 \log_{10}\left(R_x C_f\right) \tag{2}$$

where x, for the steady case, is the distance from the leading edge of the wall to the point under consideration. The value taken for x in this unsteady case is the maximum distance from the point where flow was initiated by the shock to a point where disturbances from this flow could be felt by the shock at a given location. Thus, the x distance depends on the location of the measuring station and the strength of the shock for a given length of wall. (See fig. 1.) Analytically, the expression for x for the unsteady case is

$$\frac{x}{L} = \frac{u_2}{a_2}\left(\frac{u_2 + a_2}{S_1} - 1\right) \tag{3}$$

where L is the distance from the leading edge to the measuring station. Equation (3) is plotted in figure 2 as a function of shock strength.

With an appropriate assumption for the velocity profile, the boundary-layer displacement thickness is

$$\delta^* = \beta\delta \tag{4}$$

Values of β are taken from reference 3. The mass-flow loss is calculable from

$$\Delta m = \rho_2 u_2 \, \Delta A \tag{5}$$

$$\Delta m = A \, \Delta\left(\rho_2 u_2\right) \tag{6}$$

Combining equations (5) and (6) and making the result nondimensional gives

$$\Delta\left(\frac{\rho_2}{\rho_1}\frac{u_2}{a_1}\right) = \frac{\rho_2 u_2}{\rho_1 a_1}\frac{\Delta A}{A} \tag{7}$$

With the approximation

$$\Delta A = D\delta^* \tag{8}$$

equation (7) may be combined with equations (4) and (8), yielding

$$\Delta\left(\frac{\rho_2 u_2}{\rho_1 a_1}\right) = \frac{\rho_2 u_2}{\rho_1 a_1} \beta\delta \frac{D}{A} \tag{9}$$

From a plot of the theoretical mass flow as a function of shock strength (fig. 3), the defect in shock strength can be found directly.

For the rough-wall case, the problem resolves itself into finding the boundary-layer thickness as a function of x. From the boundary-layer momentum equation for a flat plate,

$$c_f = 2 \frac{d\theta}{dx} \tag{10}$$

Letting

$$\frac{\delta}{\theta} = \eta \tag{11}$$

and

$$\frac{d\theta}{d\delta} = \frac{\theta}{\delta}$$

and combining equations (10) and (11) yields

$$c_f = \frac{2}{\eta} \frac{d\delta}{dx}$$

or

$$d\delta = \frac{1}{2} \frac{\delta}{\theta} c_f \, dx \tag{12}$$

From reference 2, for fully developed turbulent flow over very rough plates,

$$c_f = \left(\frac{1}{A + B \log_e \frac{\delta}{k}} \right)^2 \tag{13}$$

where A and B are constants depending on the form of the roughness (see refs. 2 and 4).

Combining equations (12) and (13), letting

$$dx = u_2 \, dt \tag{14}$$

and changing the dependent variable to δ/k gives

$$\left(A + B \log_e \frac{\delta}{k} \right)^2 \frac{d\delta}{k} = \frac{u_2}{2k} \frac{\delta}{\theta} \, dt \tag{15}$$

Integrating equation (15) yields

$$\frac{\delta}{k} \left[A^2 - 2B(A - B) + 2B(A - B) \log_e \frac{\delta}{k} + B^2 \log_e{}^2 \frac{\delta}{k} \right] = \frac{u_2 t}{2k} \frac{\delta}{\theta} \tag{16}$$

Equation (16) is plotted in figure 4 for two sets of constants.

Using the same x/L relationship developed for the smooth-wall case, there is a particular value of δ/k corresponding to each shock strength. With a suitable assumption for the velocity profile, the loss in shock strength may be found from equation (9) and figure 3. A step-by-step procedure in calculating the shock attenuation would alter the results by less than 2 percent for the range of shock strengths investigated.

The coordinate system used for the rough plates is shown in figure 5. The position of $y = 0$ was taken at $k/3$, as a smooth wall at that height would give the same effective cross-sectional area.

The method of calculation for the determination of the velocity profile and thickness of the boundary layer by the bullet technique will now be discussed. (See fig. 6.)

The method depends upon the assumptions that the wave strength just outside the boundary layer is maintained throughout the boundary layer and that there is no transfer of heat throughout the boundary layer. The first assumption should be valid for very weak waves regardless of the local boundary-layer conditions, while the validity for finite waves would depend upon density and velocity gradients in the boundary layer but would probably be evidenced by reflections of the wave. The second assumption is necessary in the absence of any knowledge of the boundary-layer temperature distribution but should again be valid in the lower subsonic range of stream velocities.

From the first assumption the normal Mach number of the flow relative to the bullet wave is constant, and therefore

$$M_n = M_T \sin \alpha_2 = \frac{u + u_b}{a} \sin \alpha \tag{17}$$

where

$$M_T = \frac{u_2 + u_b}{a_2} \tag{18}$$

From the second assumption, and for the case of air near room temperatures,

$$5a_w^2 = u^2 + 5a^2 = u_2^2 + 5a_2^2 \tag{19}$$

Solving equations (17) to (19) simultaneously for u yields

$$\frac{u}{u_2} = \frac{u_b}{u_2} \frac{5 \sin^2\alpha}{M_n^2 + 5 \sin^2\alpha} \left[-1 \pm \sqrt{\frac{M_n^2}{5 \sin^2\alpha} \left(\frac{u_2^2 + 5a_2^2}{u_b^2} \frac{M_n^2 + 5 \sin^2\alpha}{5 \sin^2\alpha} - 1 \right)} \right] \tag{20}$$

With the bullet velocity and stream-flow quantities in the shock tube determinable, the solution is then completed with measurements of α in the stream and in the boundary layer.

TEST METHODS AND EQUIPMENT

The shock tube was a rectangular tube of 4- by $7\frac{1}{2}$-inch cross section, 20 feet long, which could be evacuated or pressurized to 100 pounds per square inch. The arrangement of the shock tube and auxiliary equipment is shown in figures 7 and 8. The roughness was located on all four walls of the particular shock-tube section used. The roughness consisted of rows of 45° right pyramids machined at 45° angles with the flow and with the light beam through the window section. The pyramids were machined in plastic sheets which lined the tube walls, with the leading edges of the rough sheets faired and bonded to the tube wall. The sheets were made easily removable to facilitate the use of various heights of roughness. The location of the measuring gages in a small interchangeable section allowed data to be taken at various stations along the tube.

Pressure and velocity measurements were taken of the shock wave at 5- and 13-foot distances from the diaphragm. The 5-foot station determined the shock strength before entering the roughness, while the 13-foot station determined the shock strength as it came out of the roughness. Piezoelectric gages mounted in the tube wall, along with electronic chronographs, were used for measuring the velocity, while capacitance gages were used to measure pressures.

The sheets of roughness produced a change of 13 percent in the effective cross-sectional area of the 8-foot test section. Three heights of roughness were tested, pyramid heights of 1/4, 1/8, and 1/16 inch, but the effective-area change was kept constant. In addition, a set of smooth wood walls of equal area blockage was installed in the 8-foot section so that the effects of this blockage could be resolved by comparison with the smooth-wall data.

The optical investigations were carried out in a small interchangeable section with $7\frac{1}{2}$- by 16-inch windows, and this optical section along with the schlieren equipment could be located at various positions along the shock tube. For optical studies, a strip of roughness was placed on one wall of the window section and the roughness section was not used.

Two methods were introduced to study the boundary layer, a reflected shock technique and a bullet technique. The use of the reflected shock from the end wall of the tube permitted rough visual estimation of the

boundary-layer thickness by presuming that the change in curvature of the shock coincided with the outer edge of the boundary layer.

The use of a bullet fired upstream and synchronized with the shock allowed for evaluation of both thickness and velocity distribution in the boundary layer by studying the changes in slope of the wave from the bullet nose as it propagated through the boundary layer. By regulating the speed of the bullet (adjusting the amount of powder used) the wave propagated into the layer was maintained at a speed slightly supersonic with respect to the wall velocity of sound. By firing small bullets relatively far from the wall the wave was held as close to a sound wave as possible. If the wave was finite, however, the picture could still be interpreted if the strength of the wave could be assumed constant through the boundary layer.

The tests were conducted with P_1 = 1 atmosphere for shock strengths $\frac{P_2}{P_1} = 1.6$ to $\frac{P_2}{P_1} = 2.5$ and with P_1 = 0.1 atmosphere for shock strengths of $\frac{P_2}{P_1} = 2.5$ to $\frac{P_2}{P_1} = 5.8$. Varying P_1 as well as P_o enabled a large range of shock strengths and Reynolds numbers to be studied.

RESULTS AND DISCUSSION

Attenuation Measurements

The experimentally determined shock attenuations at a station 13 feet from the diaphragm are plotted as functions of shock strength for lengths of 8 feet and 4 feet of roughness, for roughness heights up to $\frac{1}{4}$ inch, in figures 9 and 10. These results are cross plotted in figures 11 and 12 to show the dependence of the attenuations on roughness height. Typical pressure records are presented in figure 13 of shocks after traveling through 8 feet of $\frac{1}{4}$-inch roughness. Because measurements of shock speed are more accurate than pressure measurements of this type, the pressure measurements were used mainly to show the quality of the pressure field behind the shock wave, rather than for measurement of the shock strength. Attenuation measurements using the wood filler strip are not plotted here since they were essentially the same as for the smooth case. Also, the results are not presented as functions of Reynolds number since no dependence on this parameter was noted in the measurements for the range of Reynolds numbers covered $\left(\frac{R_x}{L} = 1.6 \times 10^5\right.$

to 11×10^5 for P_2/P_1 of 1.6 to 2.5; $\frac{R_x}{L} = 1.1 \times 10^5$ to 6.3×10^5 for P_2/P_1 of 2.5 to 5.8).

Boundary-Layer Measurements

Photographs illustrating the use of the reflected shock and the bullet wave to show the boundary layer are presented in figures 14 and 15, as well as a photograph taken of an open jet used to confirm the method. The reflected-shock pictures are of academic interest only, since the distortion of the wave at the wall is a function of past events as well as present because the speed of the upstream wave is subsonic with respect to the wall velocity of sound. Since, in the case of the bullet wave, the wave speed (that is, bullet speed) is held supersonic with respect to the wall velocity of sound, the distortion of the wave represents only that due to propagation through the boundary layer at that point. A typical set of measurements of the change of wave angle in propagating through the boundary layer is presented in figure 16.

By using the previously outlined method of equation (20) the velocity distributions were calculated, and a typical one is shown in figure 17. Figure 18 presents the results of all the boundary-layer thickness measurements by this method as a function of distance from the leading edge of the roughness. The averages of the velocity-profile power are also presented. The scatter of points in figure 18 at $x = 3$ feet is probably due to the influence of the weak cylindrical waves in the flow on the bullet wave. These disturbances are diffractions which originated from the initial travel of the shock-tube shock wave over the roughness (see fig. 19). In some of the photographs for $x = 1$ foot these waves were present in the boundary layer and those photographs were therefore disregarded; however, at $x = 3$ feet the waves were so weak that they were not always discernible.

Theoretical Values of Attenuation

From figures 4 and 18 and equation (16) it can be seen that the selection of one set of values for the constants A and B in equation (16) will not exactly satisfy the measured values of δ without using negative values of B. Because of the scatter at $x = 3$ feet the values of the constants were chosen to agree best with the values at $x = 1$ foot as well as the common assumption that $\delta = 0$ at $x = 0$. The values chosen were $A = 3$ and $B = 3$ even though the values $A = 5$ and $B = 1.8$ would not result in any serious change in the theoretical predictions. A constant value of velocity-profile power of 1/5 was

selected, based on the measured averages of close to 1/4 and the fact that tabulated values were more readily obtainable for the 1/5-power case (ref. 3). Again, no serious change of predicted attenuation would result.

It was then possible to calculate, using the method previously outlined, all the theoretical attenuations for both the smooth- and rough-wall cases. The calculations were made for the smooth-wall case using a value of $L = 13$ feet and for the rough-wall cases using values of $L = 9$ feet and $L = 5$ feet, these lengths being the pertinent ones in this method, that is, the distance from the leading edge of the wall under consideration to the point of shock-strength measurement. The theoretical rough-wall attenuations consist of the sum of the attenuation calculated for the particular rough-wall length and that calculated for the smooth-wall length. The reason for adding these values in the rough-wall case is that the measurements are made under conditions whereby contributions to the attenuation are made by both the smooth and rough walls, and either contribution calculated under the assumptions used in this method is unaltered by the presence of the other; that is, the value of δ_{max} for the 13-foot smooth-wall calculation occurs ahead of the roughness strip, while the value of δ_{max} for the rough cases occurs at a point where no flow particles with a history over smooth walls are present (see fig. 1).

A further reason for using the sum is that by representing a boundary layer by selecting its thickest point at a particular time, similar lengthwise distributions of boundary layer are assumed when comparing cases. In the case of mixed smooth and rough flow, however, it would not be suitable to use one or the other, but rather some combination of both should be used. The sum is merely the simplest combination, since they both certainly contribute to the attenuation. The theoretical attenuations are plotted in figures 9 to 12 as dashed lines.

From examination of the experimental and theoretical results it is surprising (in view of the crudeness of the theory) to note that the theoretical predictions of shock attenuation are quite good for the weaker shocks at all values of roughness height and length, but for the stronger shocks they become progressively higher as the roughness height and length are increased. The differences in the cases of the stronger shocks are very great and are not to be expected in view of the boundary-layer thickness measurements. (That is, it should be remembered that in this theoretical method the variation of shock strength is mainly a variation of effective flow length (fig. 4).)

The measured values of boundary-layer thickness at both values of roughness length fit in very nicely with the theoretical values. Also, the measurements at 1 foot of roughness and at two greatly different

shock strengths confirm the theoretical prediction of invariance with shock strength alone.

The most important fact shown by these results is that while agreement of boundary-layer measurements with theory is good for all shock strengths, and while agreement of shock-attenuation measurements with theory is good for all the shock strengths in the smooth case, the agreement of attenuation measurements for the stronger shocks in the rough-wall case is poor.

Distortions of Wave Model Not Allowed Under One-Dimensional Flow

It is quite easy to conjecture as to quantities influencing shock-tube flows which are not accounted for in this theoretical model. However, piecing the experimental evidence into the picture will eliminate many of the possible factors. For instance, if such factors as heat-transfer effects, boundary layers of cold gas flowing from the high pressure chamber, poor flow past a broken diaphragm, area changes due to a growing boundary layer or due to roughness, shock diffraction over roughness, and the influence of pressure gradients on the boundary-layer development are included in the theory, they would be expected to increase the predicted attenuations, produce second-order decreases, or produce attenuations that would not qualitatively vary as herein observed with shock strength and roughness height.

One factor which might influence the theoretical predictions and which is not easily estimated is the effect of flow time on the boundary-layer development. (See fig. 20.) Since the theory used herein is taken from steady-flow flat-plate theory by substituting an effective flow length for the product of flow velocity and effective flow time, the boundary-layer particles in the shock case have not had the flow time which would exist in either the steady or the impulsive case. However, in view of the boundary-layer measurements at the 1-foot station (fig. 18) for greatly different shock strengths, and hence flow times, and in view of the good agreement of the smooth-wall attenuations, this factor must also be considered secondary for this comparison.

Comparison of the agreement between the boundary-layer measurements and theory with the disagreement between the attenuation measurements and theory, in fact, seems to show in a very significant fashion that the marked deviations of experiment from theory are caused by factors dependent upon shock strength alone, that is, factors other than variation of effective flow length with shock strength. The boundary-layer conditions at the wall are in agreement with the theory but this fact is not made manifest in the shock strengths observed.

Examination of equations (9) and (16) shows that the factors in the theory for rough walls influencing the shock attenuation are

$$\text{Attenuation} = f\left(x,\ k,\ M_2,\ N,\ \frac{D}{A}\right)$$

since

$$\beta = f\left(M_2,\ N\right)$$

and

$$\eta = f\left(M_2,\ N\right)$$

Boundary-layer measurements have ruled out all these parameters as causes of the discrepancy.

The most logical source of error would seem to rest in the assumption that the rate of transfer of intelligence from the boundary layer to the shock is $u + a$. This rate is a function of shock strength only and would not always apply under the assumptions of the attenuation theory used herein, particularly at the stronger shock and larger roughness values. That is, in cases where the boundary-layer thickness (not displacement thickness) is of the order of the significant shock-tube dimensions, transfer of intelligence at the assumed rate of $u + a$ would no longer be valid, since this quantity would no longer be propagated at this assumed rate. The boundary layer does, in fact, almost fill the tube for the stronger shock and larger roughness values.

Figure 21 shows the parameters which would distort this assumed one-dimensional picture. The speed of transfer at the wall would be a_{2_w}, which is always less than S_1. The speed of transfer in the stream $u_2 + a_2$ is, of course, always greater than S_1, so that the thickness of the boundary layer would determine the defect of transfer rate for a given shock strength. It can be seen, then, that the possibility that the speed of transfer will approach the value of S_1 might be very real at the thickest boundary-layer values. Figure 9 indicates those values of shock strength for the $\frac{1}{4}$- and $\frac{1}{8}$-inch roughness heights, for $L = 9$ feet, at which the boundary layer actually fills the shock tube according to the theory. Boundary-layer measurements in figure 18 confirm this fact.

The pressure records shown in figure 13 at a low and a high value of shock strength show qualitatively the fact that in the case of the stronger shock a train of expansion waves trails the shock. The curve of y'/g shown in figure 21 is included to show the effect on transfer of intelligence due to the two-dimensional aspect of the origin of the waves from the mass sink at the wall. It is not felt that this is of major importance, however, in this shock tube.

It seems clear, therefore, that the defect in rate of intelligence transfer due to thick boundary layers is the primary cause for the deviations of experimental from theoretical rough-wall shock attenuations in this shock tube.

Langley Aeronautical Laboratory,
National Advisory Committee for Aeronautics,
Langley Field, Va., June 16, 1953.

Paul W. Huber
Aeronautical Research Scientist

Donald R. McFarland
Aeronautical Research Scientist

Philip Levine
Aeronautical Research Scientist

Approved:

John V. Becker
Chief of Compressibility Research Division

ecc

REFERENCES

1. Donaldson, Coleman duP., and Sullivan, Roger D.: The Effect of Wall Friction on the Strength of Shock Waves in Tubes and Hydraulic Jumps in Channels. NACA TN 1942, 1949.

2. Von Kármán, Th.: Turbulence and Skin Friction. Jour. Aero. Sci., vol. 1, no. 1, Jan. 1934, pp. 1-20.

3. Tucker, Maurice: Approximate Turbulent Boundary-Layer Development in Plane Compressible Flow Along Thermally Insulated Surfaces With Application to Supersonic-Tunnel Contour Correction. NACA TN 2045, 1950.

4. Schlichting, H.: Experimental Investigation of the Problem of Surface Roughness. NACA TM 823, 1937.

NACA-Langley - 6-30-53 - 50

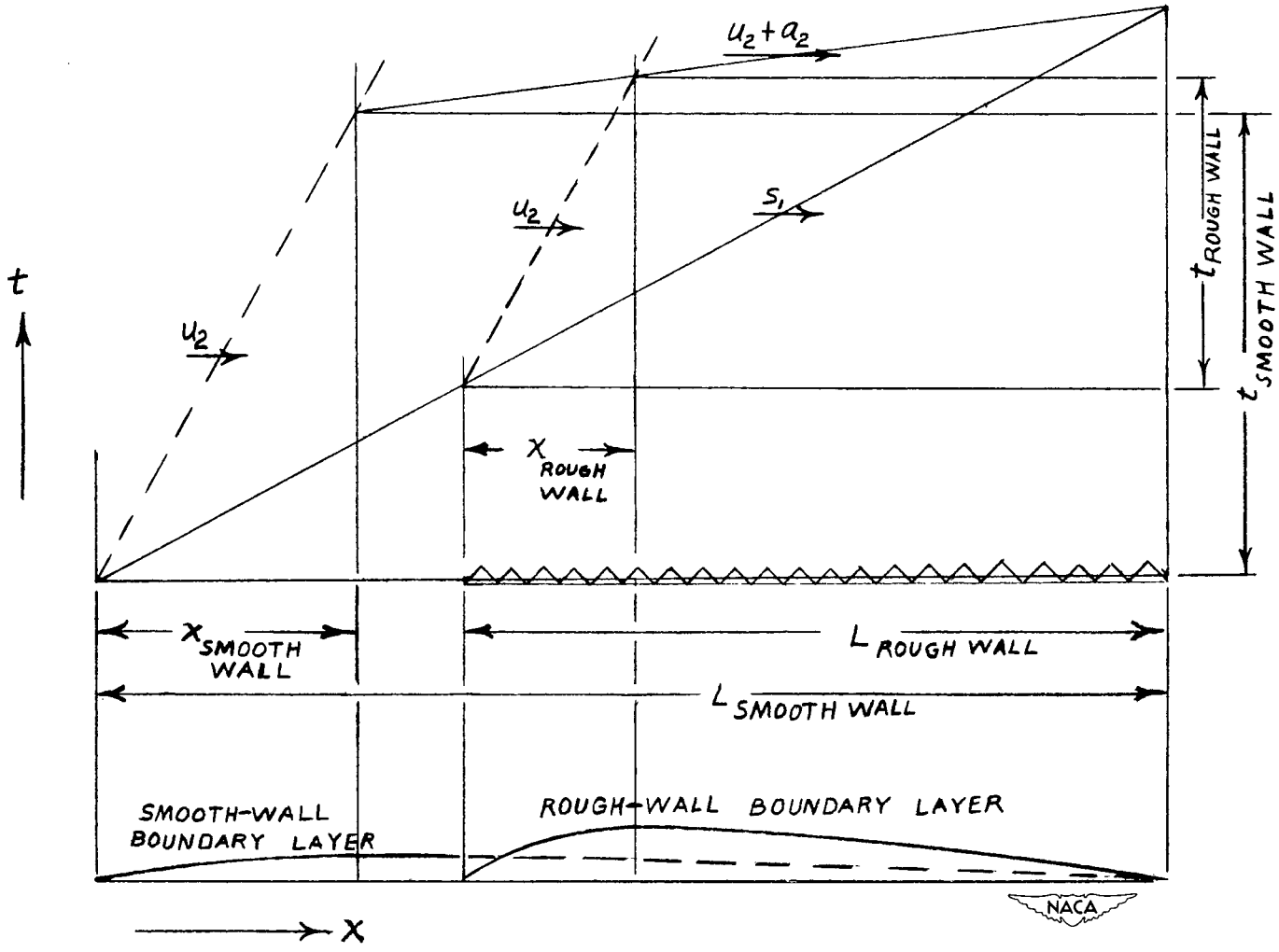

Figure 1.- Distance-time diagram used for theoretical calculations, showing contributions of smooth and rough walls to the measured attenuations.

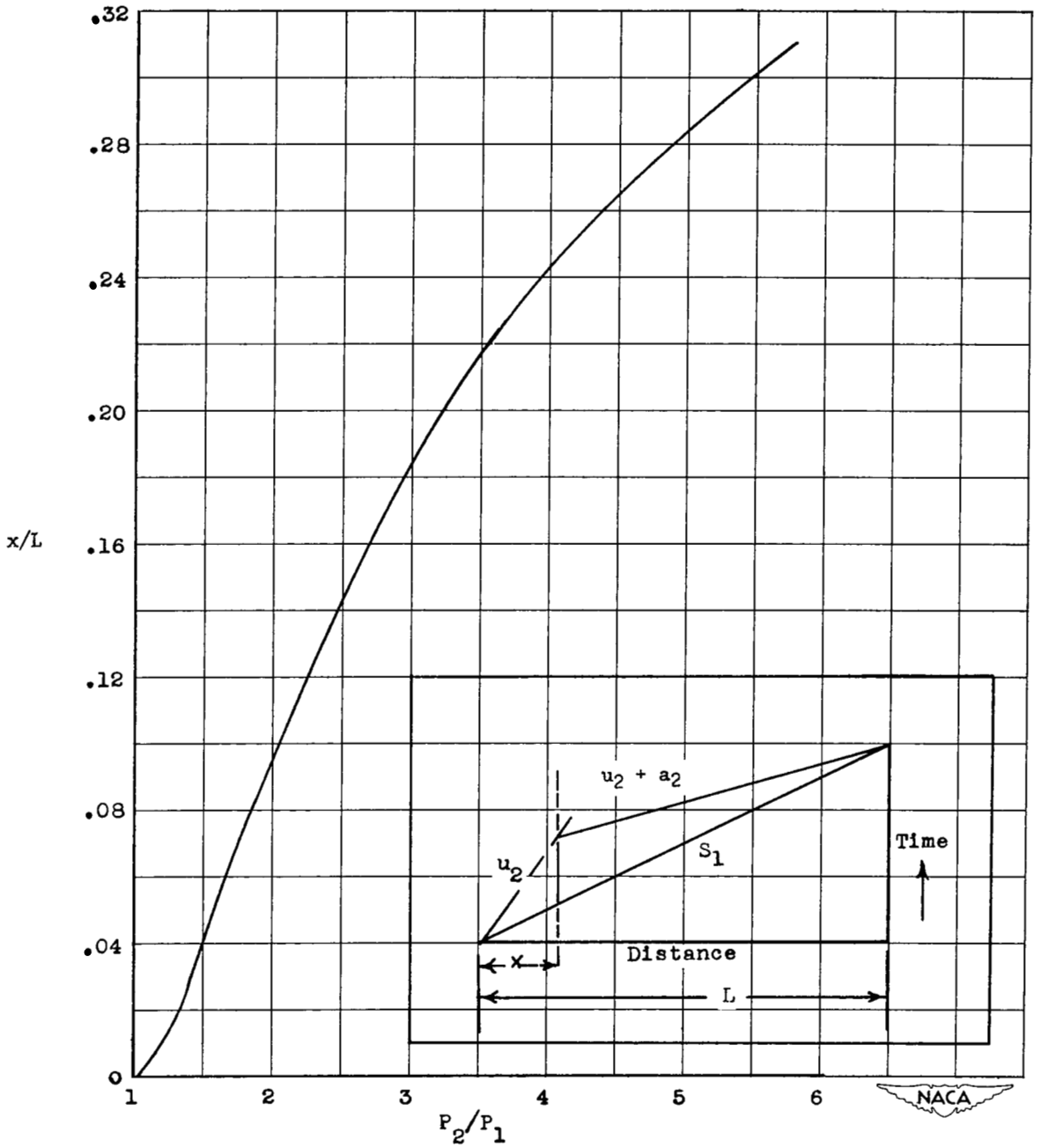

Figure 2.- Effective length of wall as a function of shock strength.

$$\frac{x}{L} = \frac{u_2}{a_2}\left(\frac{u_2 + a_2}{S_1} - 1\right).$$

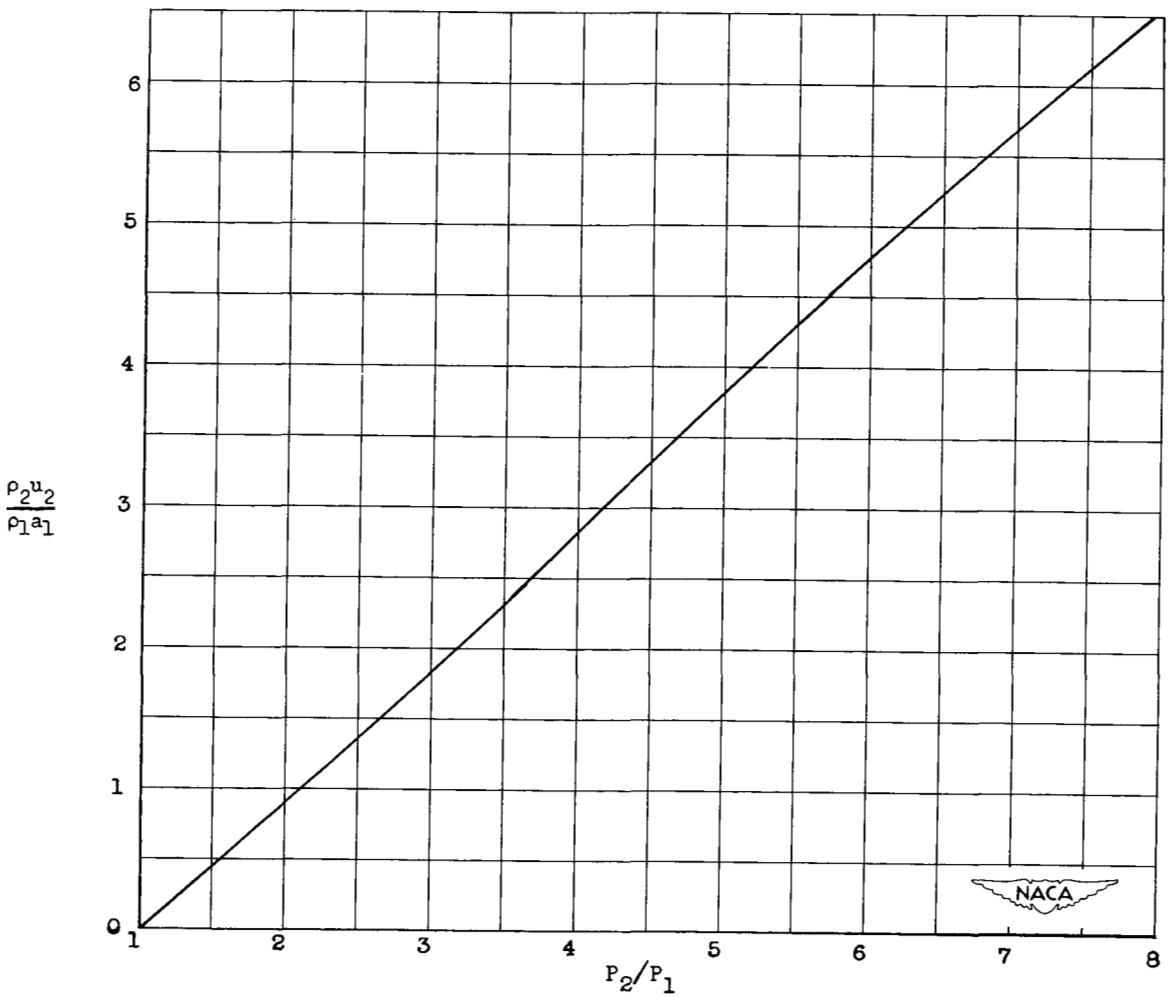

Figure 3.- Mass-flow rate across shock as a function of shock strength.

$$\Delta \frac{P_2}{P_1} = \frac{d \frac{P_2}{P_1}}{d \frac{\rho_2 u_2}{\rho_1 a_1}} \sigma, \text{ where } \sigma = \frac{\rho_2 u_2}{\rho_1 a_1} \delta^* \frac{D}{A}.$$

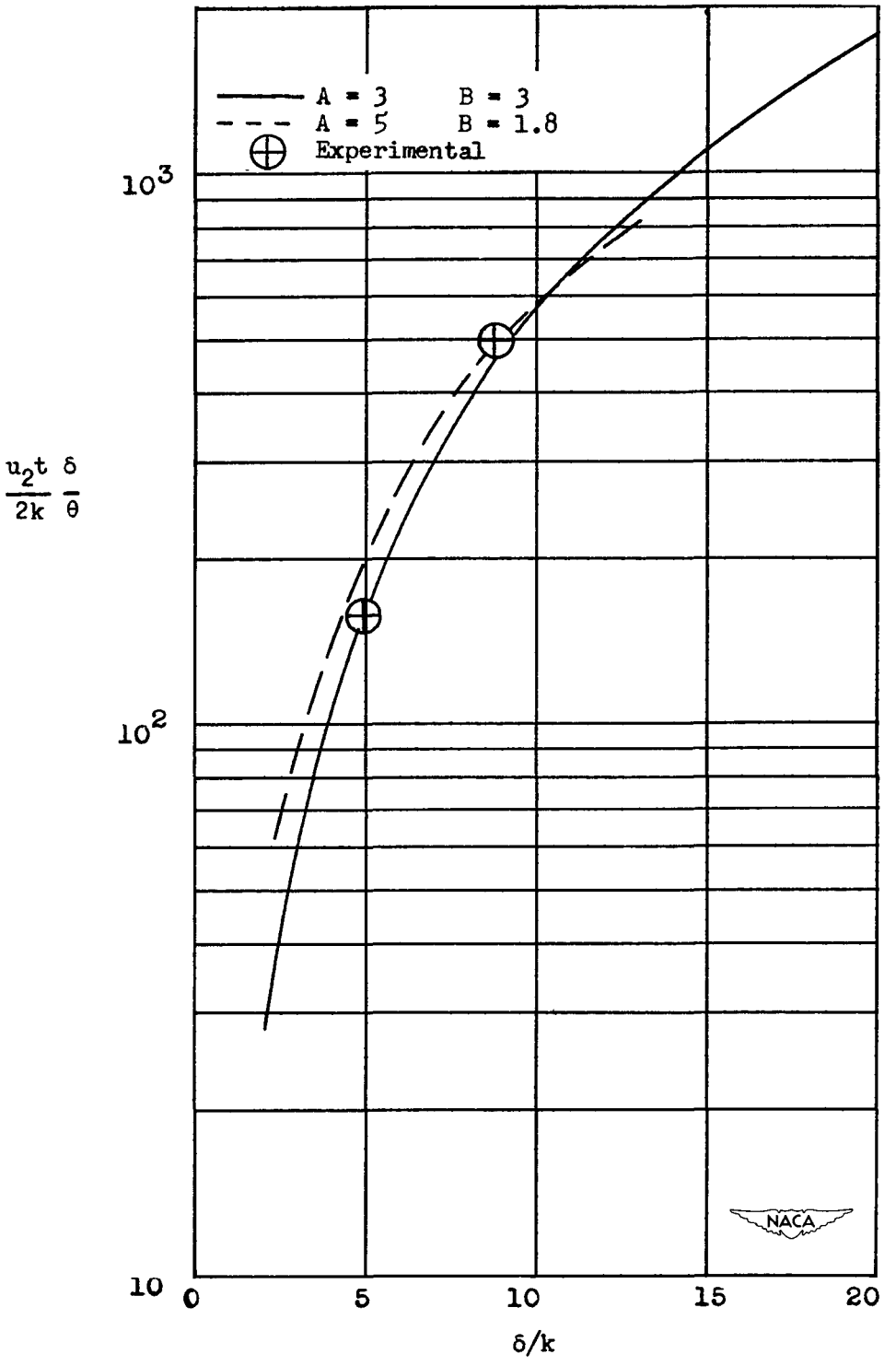

Figure 4.- Comparison of experimental boundary-layer heights with Von Kármán theory. $\frac{u_2 t}{2k} \frac{\delta}{\theta} = \frac{\delta}{k}\left[A^2 - 2B(A - B) + 2B(A - B)\log_e \frac{\delta}{k} + B^2 \log_e{}^2 \frac{\delta}{k}\right]$.

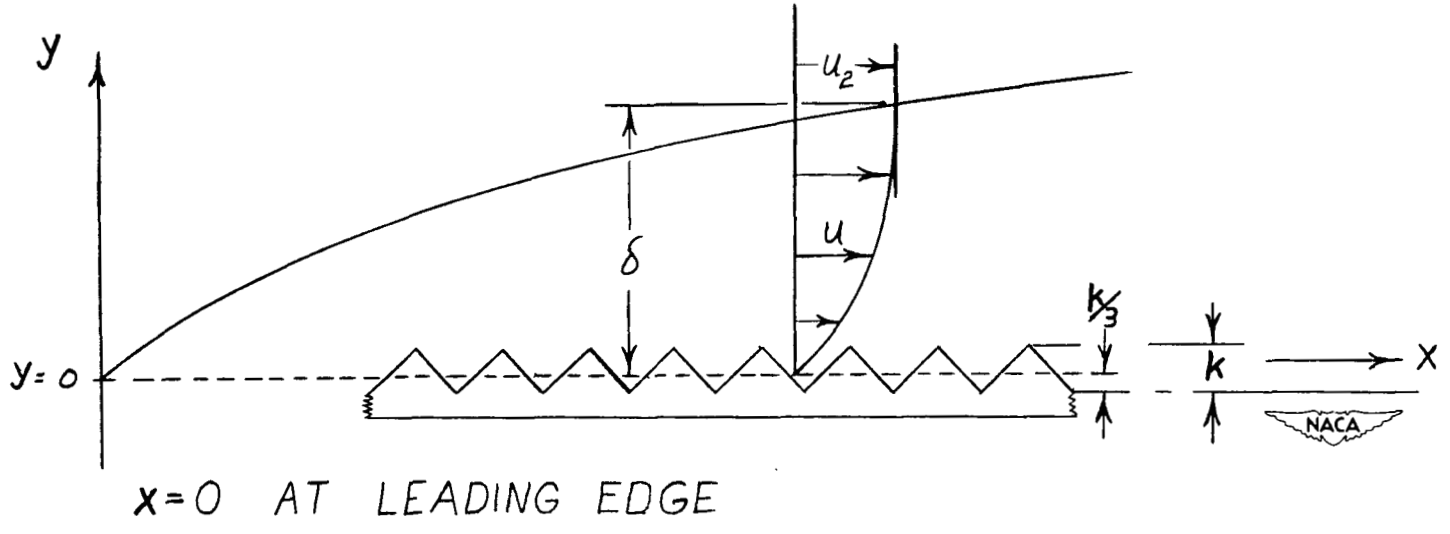

Figure 5.- Location of coordinates for rough plates.

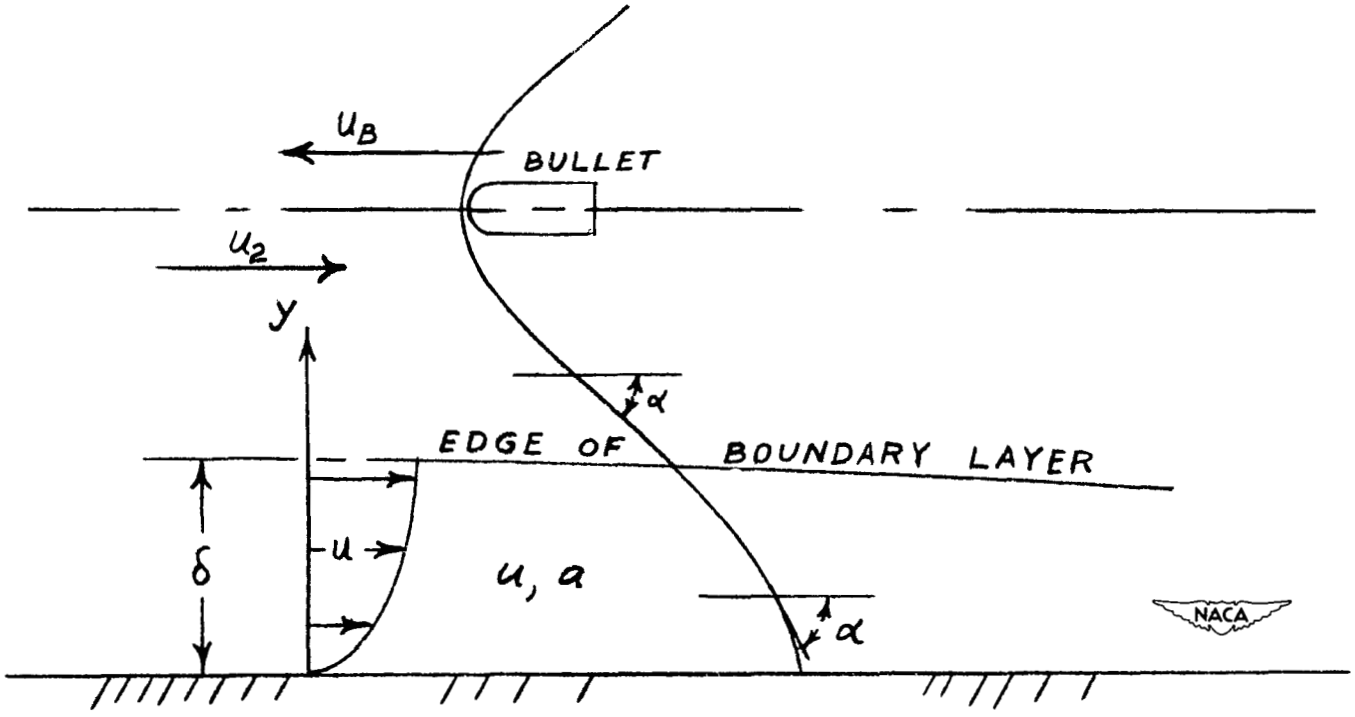

Figure 6.- Bullet method for determining a velocity profile from a weak wave. $\frac{M_h}{\sin \alpha} = \frac{u_B + u}{a}$; $\frac{u}{u_2} = \sqrt{\frac{a_{2_w}^2 - a^2}{a_{2_w}^2 - a_2^2}}$.

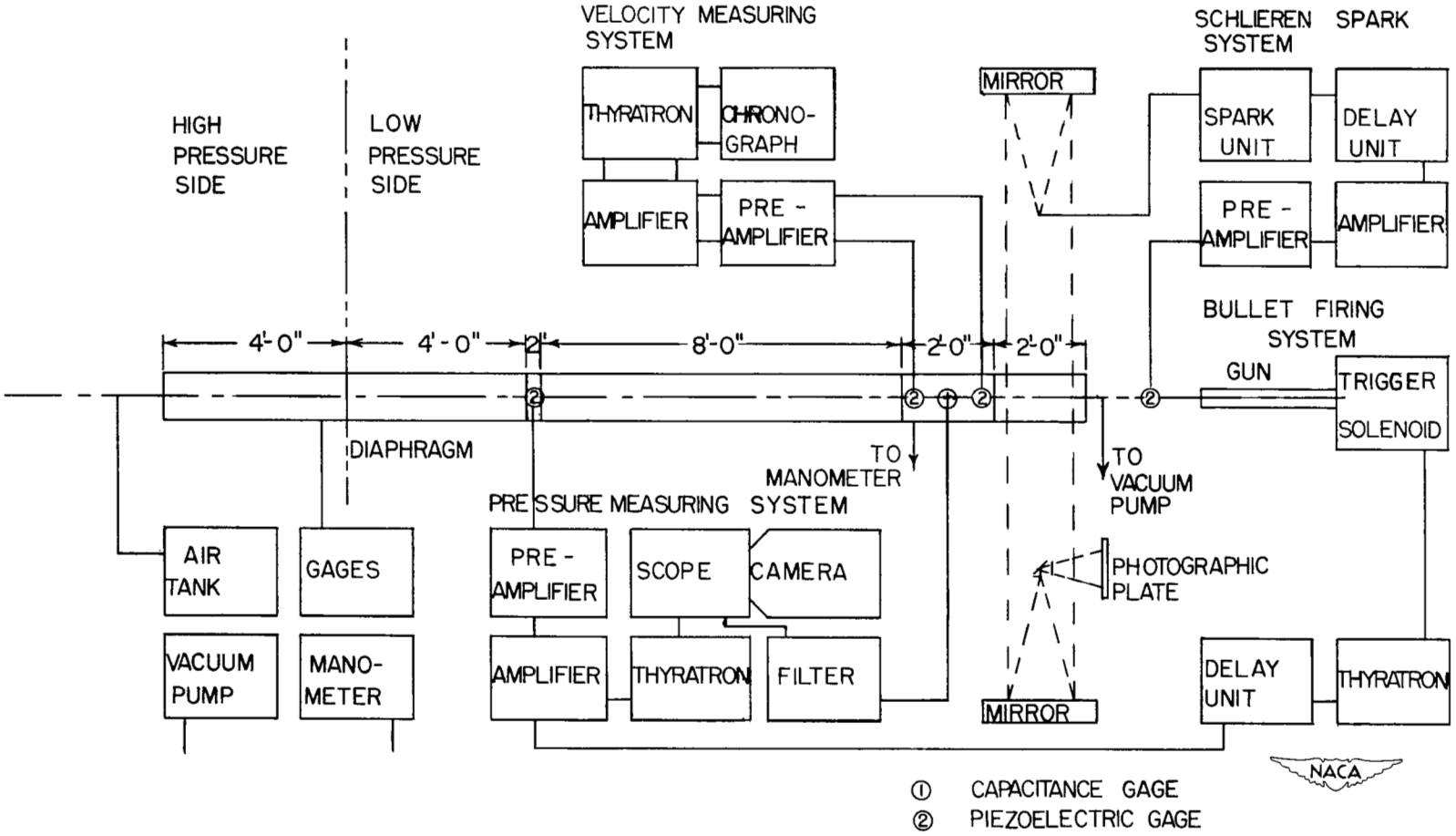

Figure 7.- Arrangement of shock tube and instrumentation.

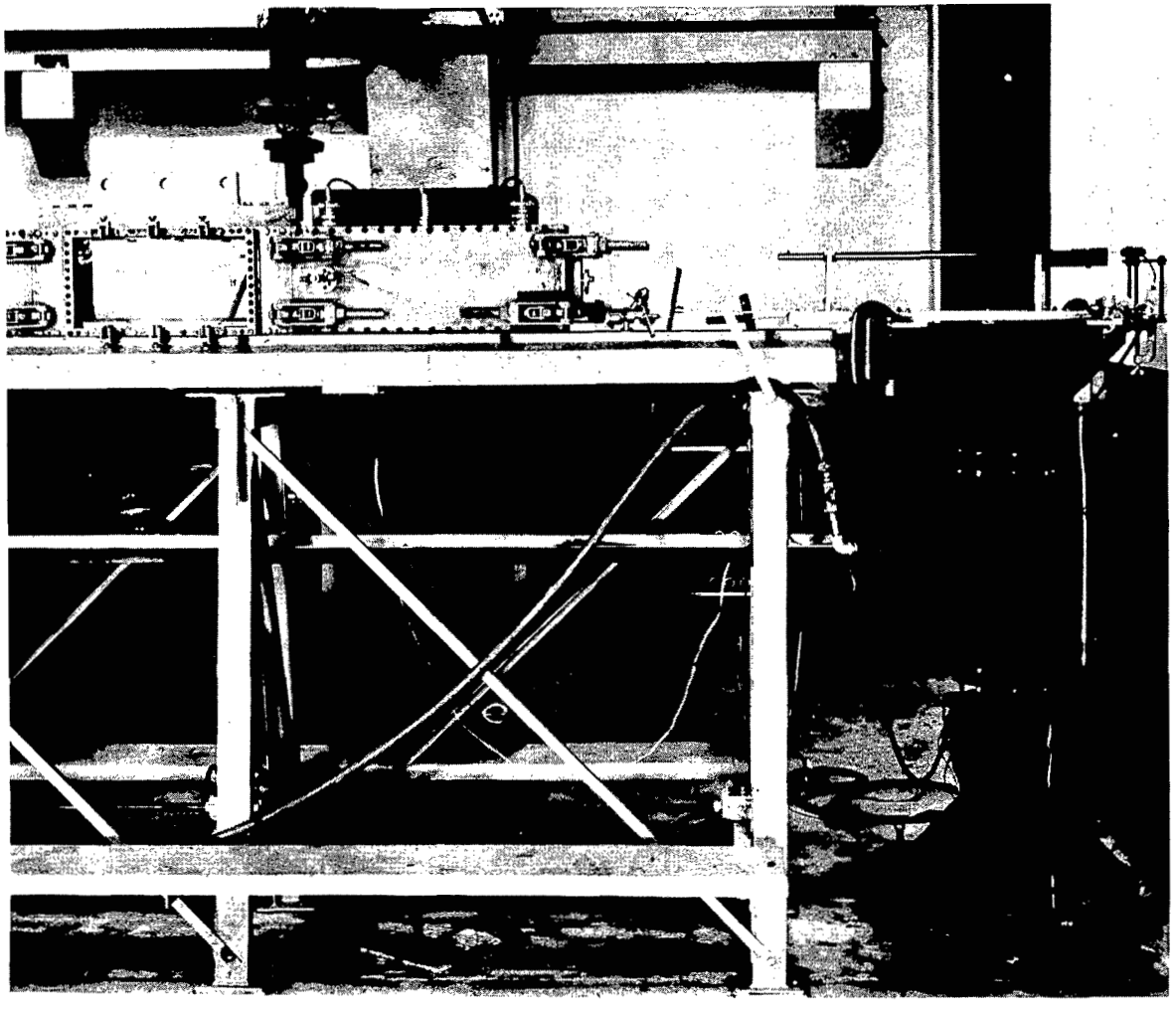

L-79642

Figure 8.- View of shock-tube window section, measuring section, and bullet-firing mechanism.

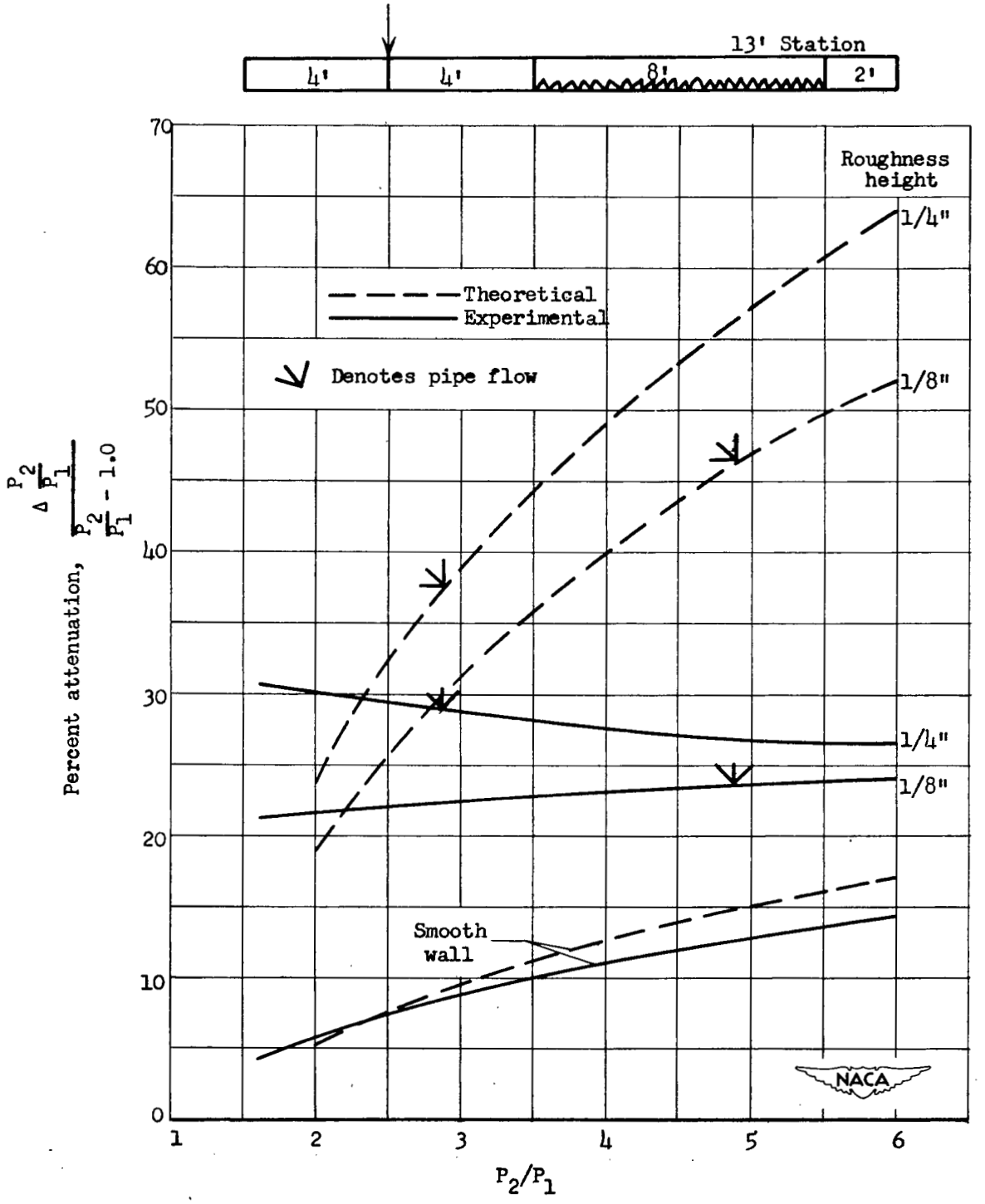

Figure 9.- Comparison of experimental and theoretical shock attenuations for 8 feet of roughness as functions of shock strength.

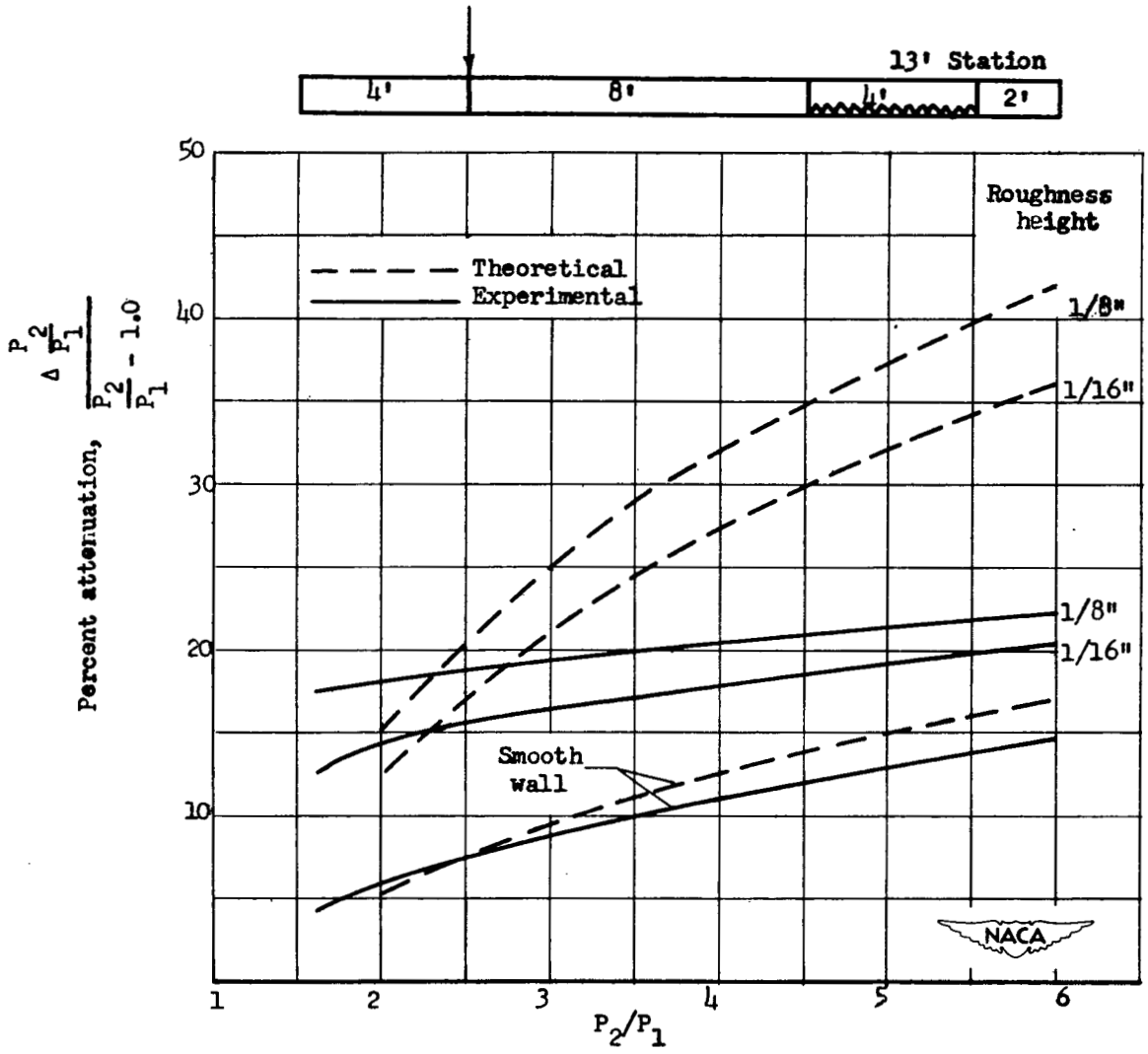

Figure 10.- Comparison of experimental and theoretical shock attenuations for 4 feet of roughness as functions of shock strength.

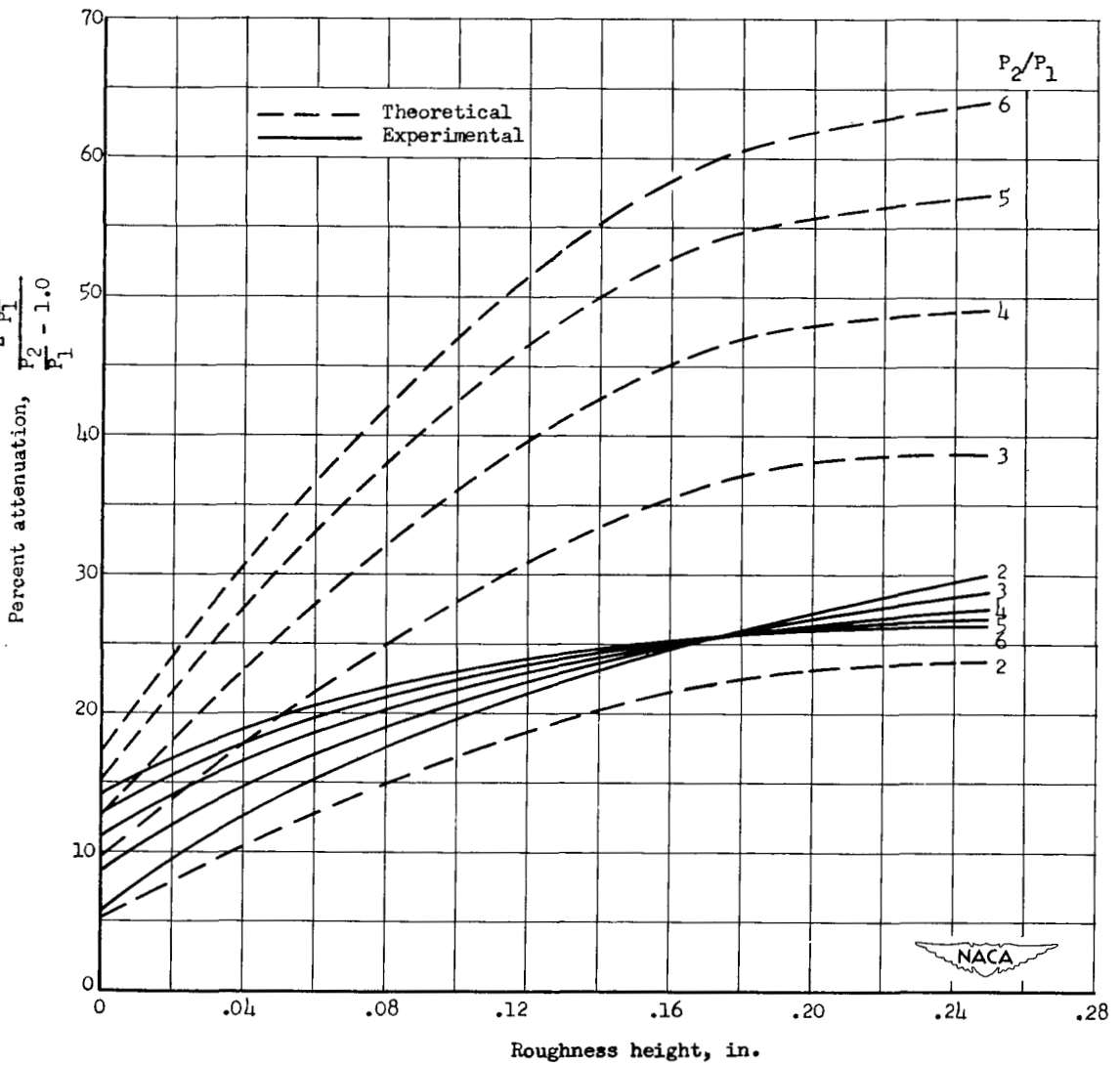

Figure 11.- Comparison of experimental and theoretical shock attenuations for 8 feet of roughness as functions of roughness size.

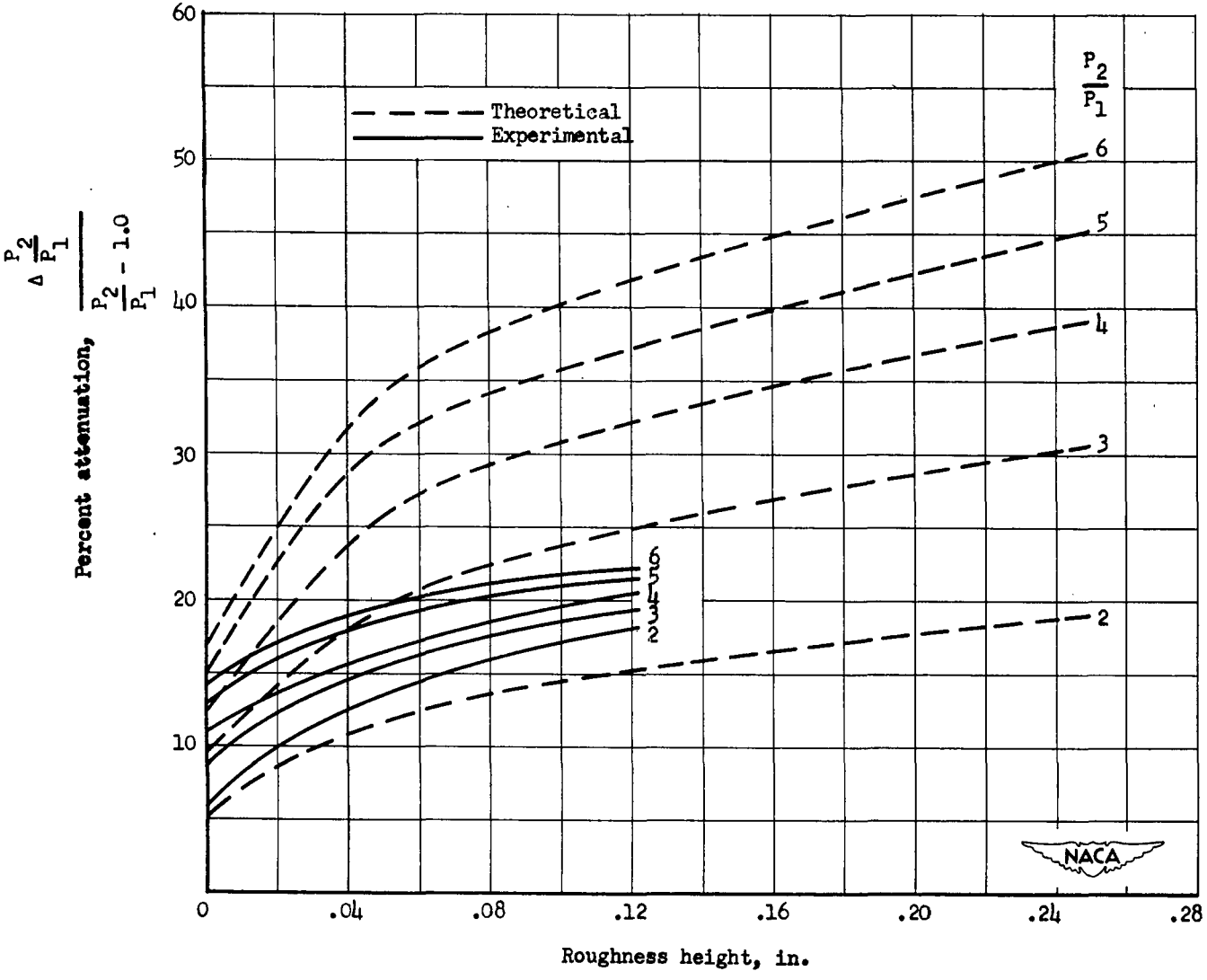

Figure 12.- Comparison of experimental and theoretical shock attenuations for 4 feet of roughness as functions of roughness size.

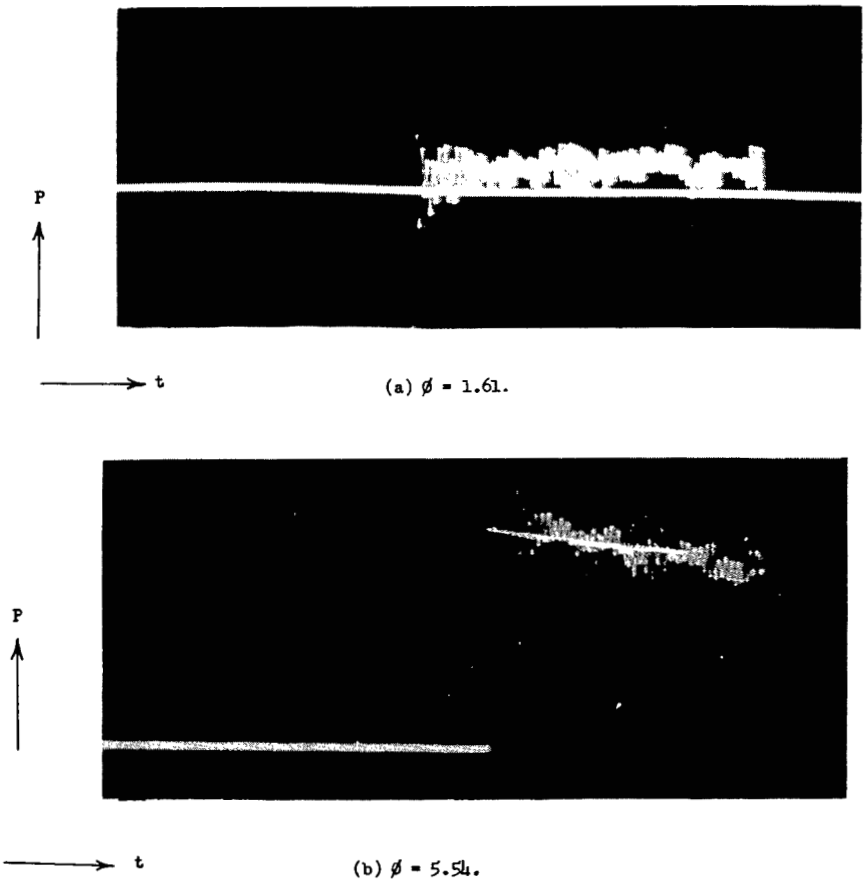

L-80228

Figure 13.- Typical pressure records of a weak and a strong shock after traveling through 8 feet of $\frac{1}{4}$-inch roughness to show the difference in quality of the pressure field behind the shock.

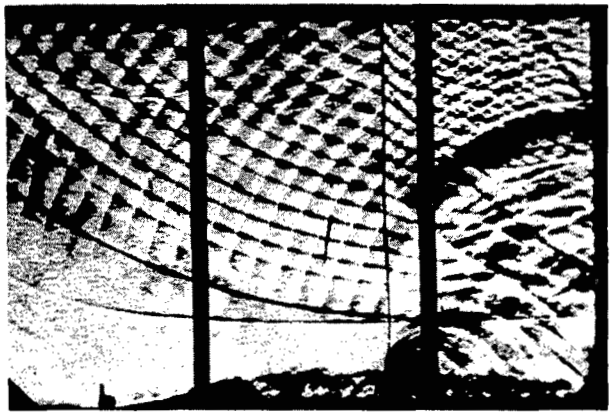

(a) $\phi = 2.$
Showing leading edge

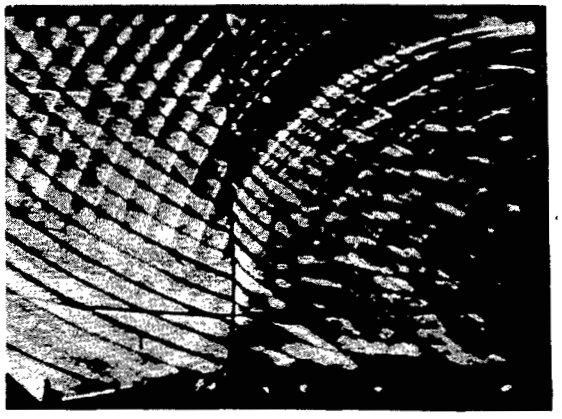

(b) $\phi = 2.$
Showing leading edge

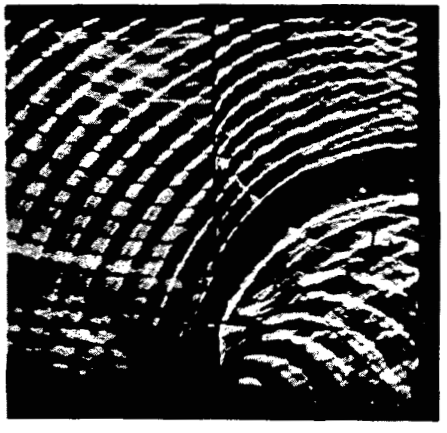

(c) $\phi = 1.6.$

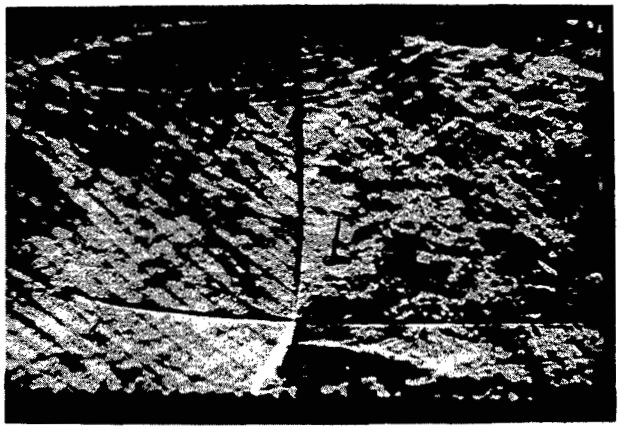

(d) $\phi = 3.5.$

L-80231

Figure 14.- Boundary-layer thickness by the reflected-shock technique.

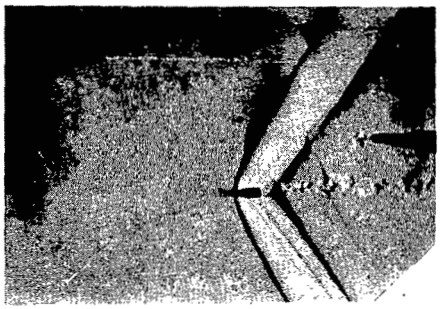

(a) Distortion of wave from service air jet located over bullet path. (No shock-tube flow.)

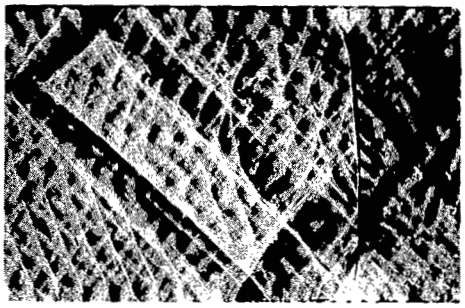

(b) 0.5 feet of rough wall; ϕ = 1.7.

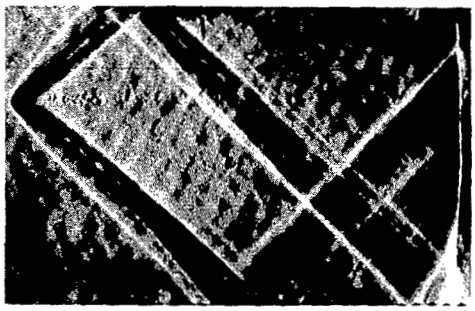

(c) 2.5 feet of rough wall; ϕ = 1.6.

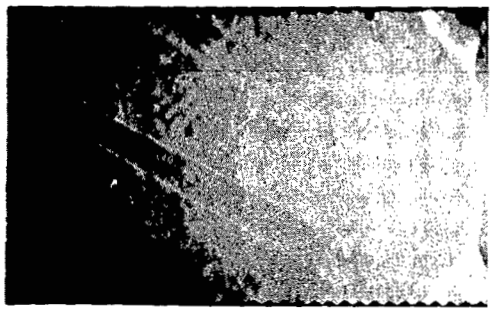

(d) 1.2 feet of rough wall; ϕ = 3.9.

L-80229

Figure 15.- The bullet technique for finding velocity profiles and boundary-layer thickness for various lengths of rough wall and shock strength.

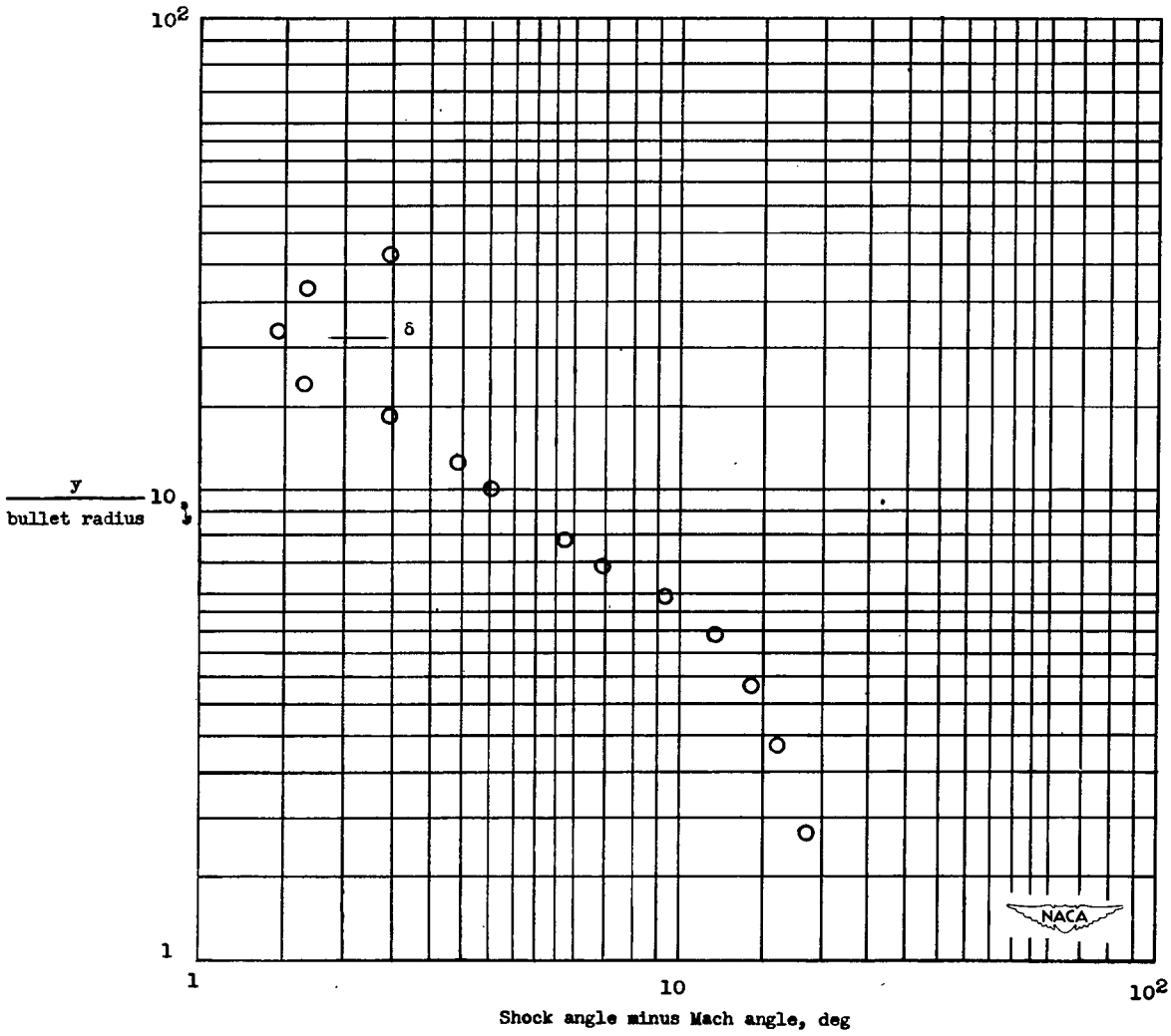

Figure 16.- Method for determination of boundary-layer height from bullet shock angles by selecting y at minimum values of shock angle.

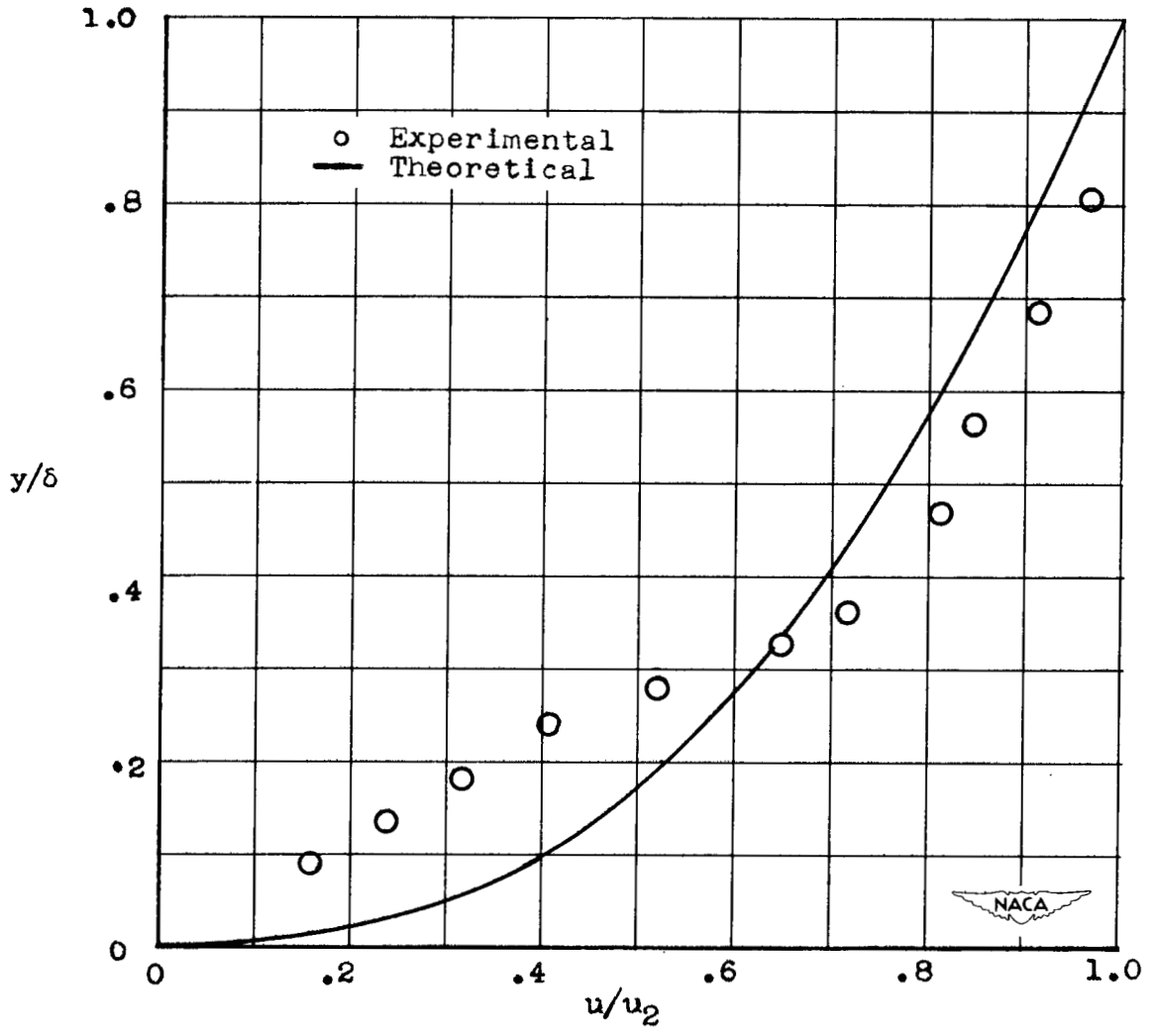

Figure 17.- Comparison of measured velocity distribution with a theoretical velocity distribution of 1/4 power.

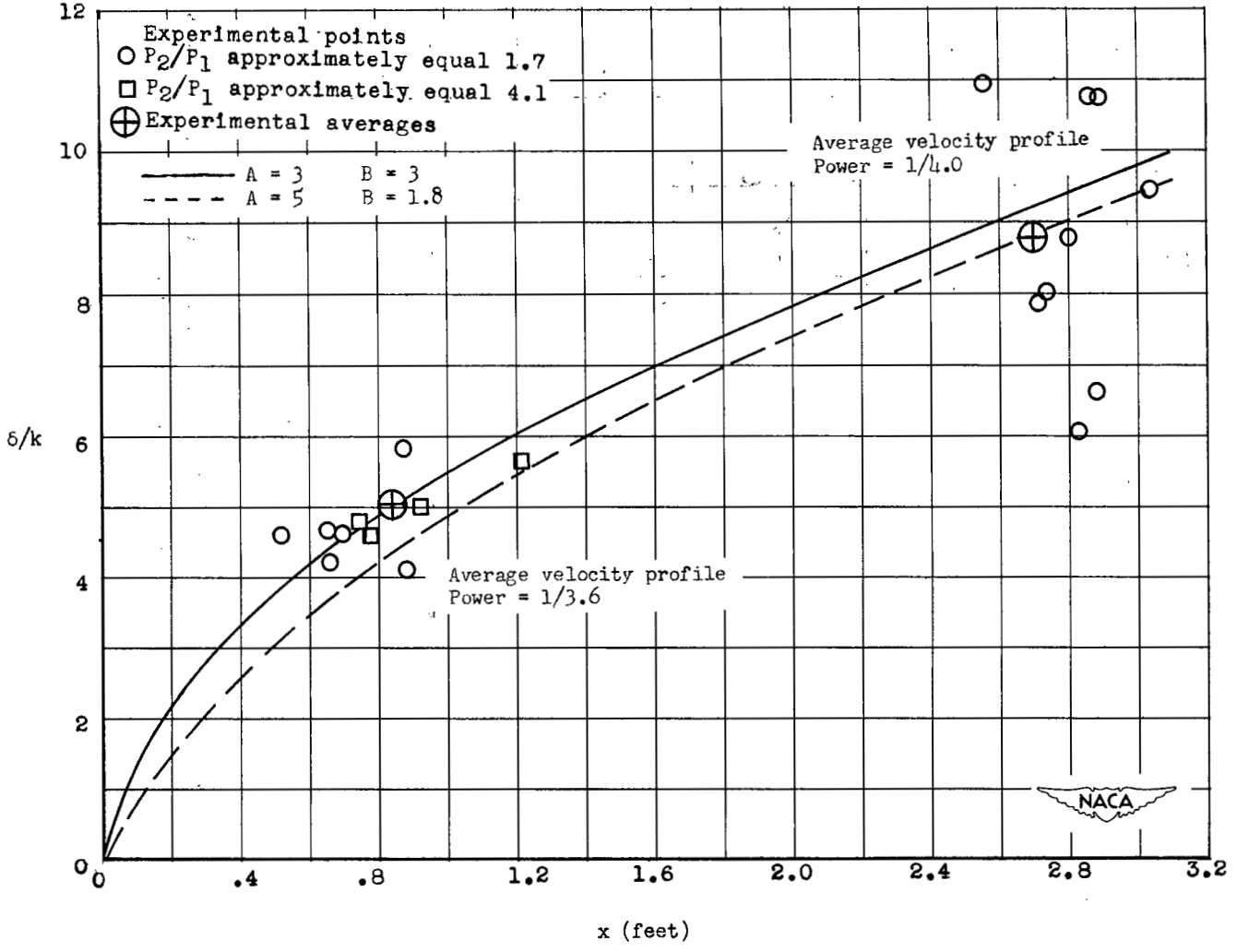

Figure 18.- Comparison of experimental boundary-layer thickness with theory. $\frac{u_2 t}{2k}\frac{\delta}{\theta} = \frac{\delta}{k}\left[A^2 - 2B(A - B) + 2B(A - B)\log_e \frac{\delta}{k} + B^2 \log_e{}^2 \frac{\delta}{k}\right]$.

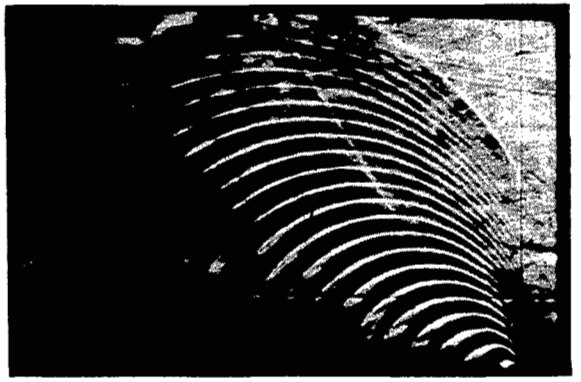

(a) ϕ = 1.4.
Showing leading edge

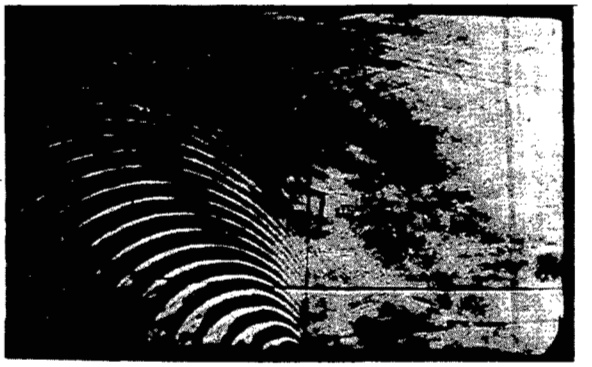

(b) ϕ = 1.5.

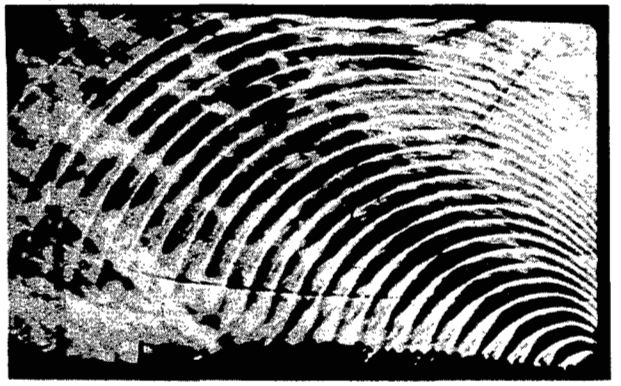

(c) ϕ = 2.
Showing leading edge

L-80232

(d) ϕ = 4.6.

Figure 19.- Disturbances and boundary-layer growth for various shock strengths.

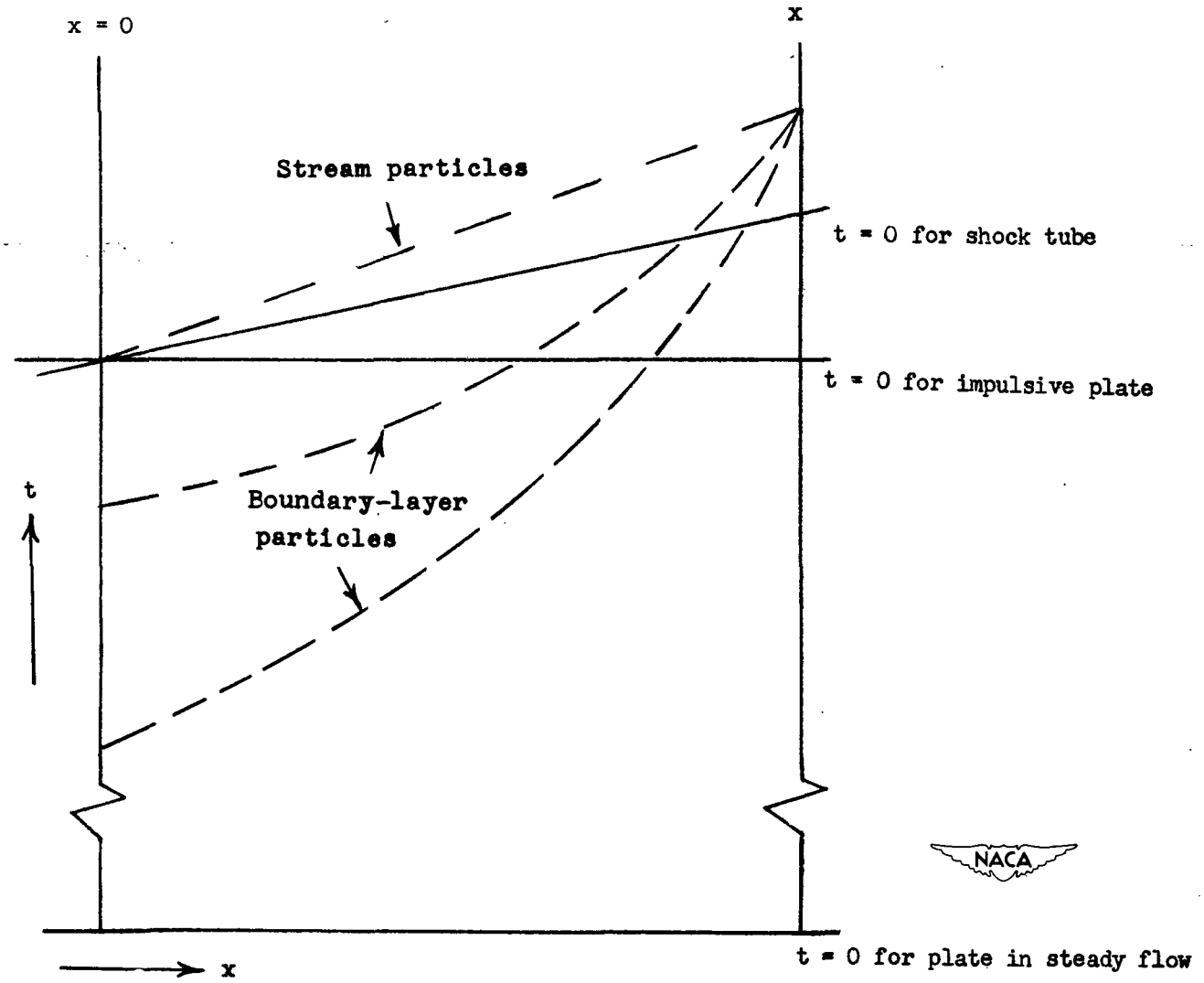

Figure 20.- Comparison of time histories of boundary-layer flow for equilibrium with wall for three cases of flow from x = 0 to x.

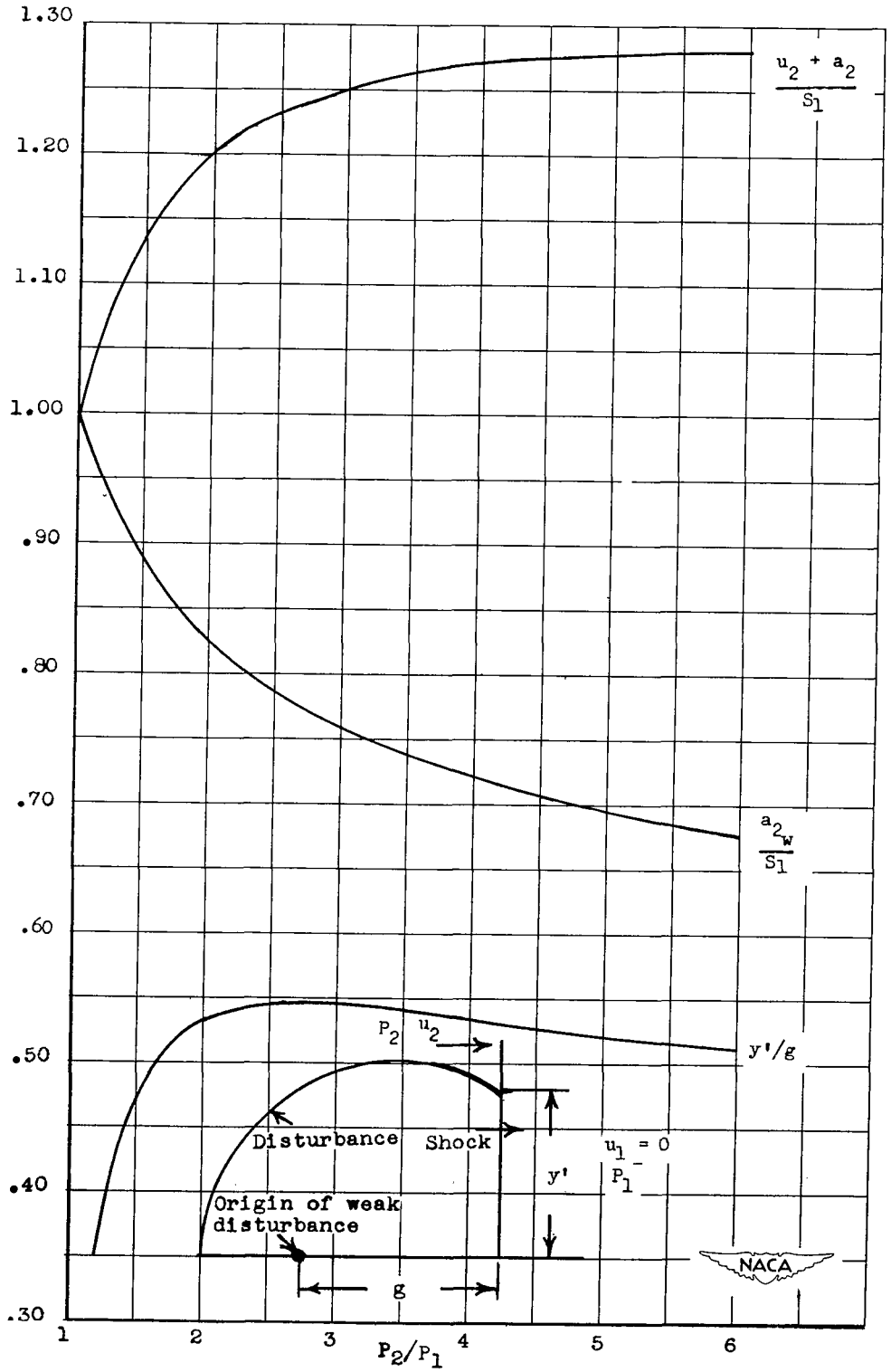

Figure 21.- Parameters influencing one-dimensional concept of intelligence transfer from boundary layer to shock.